Surface & Coatings Technology 203 (2009) 3708–3717

Contents lists available at ScienceDirect

Surface & Coatings Technology

journal homepage: www.elsevier.com/locate/surfcoat

Influence of micro-blasting on the microstructure and residual stresses of CVD κ-Al_2O_3 coatings

C. Barbatti [a,b], J. Garcia [c,d,*], R. Pitonak [e], H. Pinto [a], A. Kostka [a], A. Di Prinzio [f], M.H. Staia [f], A.R. Pyzalla [c]

[a] Max-Planck-Institut für Eisenforschung GmbH, 40237 Düsseldorf, Germany
[b] Corus Research, Development and Technology, P.O. Box 10000, 1970 IJmuiden, The Netherlands
[c] Helmholtz Zentrum Berlin fuer Materialien und Energie GmbH, 14109 Berlin, Germany
[d] Ruhr Universität Bochum, Materials Technology, 44780 Bochum, Germany
[e] R&D, Boehlerit GmbH & Co. KG, 8605 Kapfenberg, Austria
[f] School of Metallurgy and Materials Science, Universidad Central de Venezuela, P.O.Box 47885, Los Chaguaramos, 1041 Caracas, Venezuela

ARTICLE INFO

Article history:
Received 10 February 2009
Accepted in revised form 3 June 2009
Available online 17 June 2009

Keywords:
CVD
κ-Al_2O_3
Cemented carbides
Micro-blasting
Residual stresses
Synchrotron X-ray diffraction

ABSTRACT

Cemented carbides coated with CVD multilayers are commonly used in metal cutting turning and milling operations. For many applications, a micro-blasting finishing procedure based on an impact treatment of the surfaces is carried out in order to smooth the coated surface and reduce sharp cutting edges. In this work, micro-blasting with corundum in aqueous solution at pressures between 0.05 and 0.3 MPa was applied to CVD TiN/Ti(C,N)/κ-Al_2O_3 multilayer coatings deposited onto cemented carbides in order to investigate its influence on the micro-topography, microstructure and residual stresses. The results showed that the micro-blasting reduces the surface roughness and affects the coating thickness. TEM investigations revealed no significant changes on the microstructure of the κ-Al_2O_3 top layer. Synchrotron X-ray investigations showed that the residual stress state of the as-deposited κ-Al_2O_3 top layer is not affected by the micro-blasting treatment under the conditions investigated.

1. Introduction

Coated cemented carbides are commonly used in the metal cutting industry for machining of iron-base alloys. In order to increase the tool life of cutting inserts, cemented carbides are coated with wear resistant coatings by chemical vapour deposition (CVD) or physical vapour deposition (PVD).

Al_2O_3 is considered an ideal coating layer in high-speed metal cutting due to its high chemical stability, high hardness and favourable thermal properties at the high temperatures reached during metal cutting [1–3]. Due to the mixed ionic and covalent bonding, the material is highly insulating [4,5], thus being usually applied as a top layer to act as a thermal and diffusion barrier. The CVD technique is commonly employed since it is the only deposition method that allows the economical large-scale production of high-quality alumina coatings [6]. In addition to the stable α-Al_2O_3, alumina can be obtained in two other metastable modifications by CVD, namely κ-Al_2O_3 and γ-Al_2O_3 [7,8]. A typical multilayer combination is that of Ti(C,N) to provide wear resistance, followed by an Al_2O_3 top layer, which enhances the thermal resistance of the tool. Due to adhesion problems between the Ti(C,N) and the Al_2O_3 coating, the use of an intermediate layer made of Ti(C,N,O) is proposed [9,10]. These intermediate layers of Ti-based compounds favour the nucleation of κ-Al_2O_3 [11,12]. More recently, a novel method for producing an adequate bonding of the Al_2O_3 top layer onto the Ti(C,N) by the formation of a nano-transition needle-like phase arrangement has proved to be advantageous [13]. This method also leads to the formation of κ-Al_2O_3.

Micro-blasting is a finishing procedure based on an impact treatment of the surfaces. Generally, this procedure is applied to coatings to clean, smooth the surface and reduce sharp cutting edges [14–16]. This process involves the use of high pressure and abrasive powders. Besides, there is still the possibility of achieving an attractive side effect, namely, the introduction of beneficial compressive residual stresses.

Previous works showed that micro-blasting of ground and polished hard metal substrates can increase the cutting performance of coated tools mainly due to film adhesion enhancement [17–20]. Moreover, it has been recently shown that micro-blasting treatment of PVD coatings deposited on hard metal substrates improves its residual stress with regard to fatigue strength and cutting performance of the coated tool [21]. In [22,23] it is reported that compressive residual stresses were induced on PVD/CVD multilayers by micro-blasting with pressures between 0.2 and 0.6 MPa. Holzschuh reports in [24] a method to introduce compressive stresses in CVD multilayers by removing the TiN top layer of a Ti(C,N)/Al_2O_3/TiN multilayer coating by micro-blasting, however, without any mention of the blasting

* Corresponding author. Helmholtz Zentrum Berlin fuer Materialien und Energie GmbH, 14109 Berlin, Germany. Tel.: +49 234 32 28229.
E-mail address: jose.garcia@helmholtz-berlin.de (J. Garcia).

0257-8972/$ – see front matter © 2009 Elsevier B.V. All rights reserved.
doi:10.1016/j.surfcoat.2009.06.021

conditions employed. In [22–24] improvements of tool life of micro-blasted Al_2O_3 coated cutting inserts in metal cutting are presented. The reason for the increment of the tool life is reported to be related to the introduction of compressive residual stresses on the Al_2O_3 top layer. Although not mentioned in their publications, it is to be understood from the results presented that the authors worked with α-Al_2O_3 coatings.

Nevertheless, in spite of the many publications, no systematic study on the influence of micro-blasting pressure on Al_2O_3 coating is found in the literature.

In this work, we applied micro-blasting to CVD multilayer TiN/Ti(C,N)/κ-Al_2O_3 coatings. The micro-blasting pressure range varies between 0.05 and 0.3 MPa. We aim at investigating systematically the influence of the blasting pressure on the micro-topography and the possibility of inducing compressive residual stresses on the κ-Al_2O_3 top layer.

The microstructure and residual stress state of the κ-Al_2O_3 top layer were investigated for the as-deposited and micro-blasted conditions by scanning electron microscopy, transmission electron microscopy, synchrotron as well as laboratory source X-ray diffraction and roughness measurements.

2. Experimental

2.1. Substrate and coatings

The coatings were deposited onto cemented carbide substrates (90 wt.% WC–10 wt.% Co) with a size of 14 mm × 14 mm × 5 mm, produced by state-of-the-art powder metallurgy sintering techniques. A TiN/Ti(C,N)/κ-Al_2O_3 multilayer was applied on the hard metal substrate by CVD in a standard hot-wall CVD reactor working at 1015 °C and 15 kPa. The TiN and Ti(C,N) layers were deposited from the gas mixture $TiCl_4$–CH_4–N_2–H_2. The Al_2O_3 layer was deposited on top of the Ti(C,N) layer from the gas mixture $AlCl_3$–ClH_2–CO_2. Due to the deposition conditions employed, κ-Al_2O_3 was produced as a top coating layer.

2.2. Micro-blasting

After deposition, the coatings were subjected to a micro-blasting treatment performed using an injector-type system in a commercial industrial blasting furnace. Standard industrial parameters were employed. The grit blasting material used was 320-mesh (average diameter within ~50 μm) corundum shots in aqueous solution. The micro-blasting treatment was carried out for 30 s to ensure full coverage of the surfaces. The pressure was varied within the range from 0.05 MPa to 0.3 MPa in steps of 0.05 MPa.

2.3. Microscopy

Scanning electron microscopy (SEM) was performed on non-polished surfaces and fractured cross-sections. Specimens for transmission electron microscopy (TEM) analyses were prepared by using a gallium source JEOL JEM-9320 focused ion beam (FIB) system operating at 30 kV. A JEOL 2200F TEM/STEM operating at 200 kV and equipped with an EDX system was used for studying the microstructure of coatings in the as-deposited and micro-blasted state.

2.4. Roughness

The surface roughness (R_a and R_z) of as-deposited and micro-blasted coatings was determined from atomic force microscopy pictures. Four areas were measured in order to determine an average value. The measurements were carried out in a Nano-scratch tester equipped with an atomic force microscope (CSM Instruments).

2.5. Phase and residual stress analyses

In order to assess the phase constitution within the as-deposited and micro-blasted coatings, X-ray diffraction (XRD) diffractograms were obtained using synchrotron radiation at the experimental station G3 at DORIS III at HASYLAB at DESY, Hamburg. The radiation energy was 6.9 keV ($\lambda_{Co} = 1.7904$ Å). The beam size was set as 4 mm × 1 mm.

The residual stresses within the κ-Al_2O_3 coatings were determined on a laboratory four-circle diffractometer operating with Co–K_a radiation and parallel-beam geometry using the $\sin^2\psi$ method [25]. Owing to the weak macroscopic texture of the κ-Al_2O_3 coating, unrestricted lattice spacing measurements could be performed for 24 sample directions defined by the inclination angle ψ between 0° and 89.8° at the azimuths $\varphi = 0°$ and 180°. Considering the stress state in the coatings to be biaxial and of rotational symmetry, the fundamental relationship of X-ray stress analysis can be solved to provide the depth-dependence of the in-plane residual stresses $\sigma_{//}$ [26]:

$$\sigma_{//}(\tau_{\text{eff}}) = \frac{\varepsilon_\psi(\tau_{\text{eff}})}{\left(\frac{1}{2}s_2 \cdot \sin^2\psi + 2s_1\right)} \tag{1}$$

where ε_ψ is the measured lattice strain, $\sigma_{//}$ is the in-plane residual stress, τ_{eff} is the information depth, and $1/2s_2$ and s_1 are the phase-specific diffraction elastic constants (DEC).

The concept of effective information depth τ_{eff} is usually applied in diffraction studies of thin films to define the depth from which the diffraction information comes, since the penetration depth τ of the radiation into a certain material may be much larger than the film thickness. According to its definition τ_{eff} can be tuned within the film thickness by changing the ψ-angle [27]:

$$\tau_{\text{eff}} = \frac{\int_0^D z \cdot e^{-\frac{z}{\tau}} dz}{\int_0^D e^{-\frac{z}{\tau}} dz} = \tau - \frac{De^{-\frac{D}{\tau}}}{1 - e^{-\frac{D}{\tau}}} \tag{2}$$

where τ is the average penetration depth for an infinitely thick sample, which is a function of the ψ-tilt, and D is the thickness of the κ-Al_2O_3 layer. In this approach the maximum achievable information depth approaches the limit of half layer thickness ($D/2$) as the ratio D/τ in Eq. (2) decreases towards zero.

The lattice strains were measured for the {135} diffraction line of κ-Al_2O_3. This reflection was chosen based on a compromise between the ease for separating this line from neighboring ones, its intensity and the highest possible 2θ-angle. The DEC were estimated using the mechanical values of Young's modulus $E = 361.7$ GPa and Poisson's ratio $\nu = 0.24$ for κ-Al_2O_3 at room temperature available in [5].

The integral breadth of the selected reflection was also determined as a function of the micro-blasting conditions. This quantity is related to the density of crystalline defects (dislocations, stacking faults) and small size of crystallites (i.e. domains over which diffraction is coherent) [28]. The integral breadth for each condition represents an average on the results obtained at different ψ-angles by fitting the {135} diffraction lines using pseudo-Voigt functions.

3. Results

3.1. Microstructure of the as-deposited coatings

The as-deposited layer system is shown in Fig. 1. The CVD TiN/TiCN/κ-Al_2O_3 layers show good adhesion to the cemented carbides, hence no pores, brittle phase formation nor spallation between the substrate and the coating are observed. The layer thickness is homogeneous across the coating, the thickness of the TiN is of about 0.2 μm, for the intermediate Ti(C,N) layers is about 3 μm and the thickness of the κ-Al_2O_3 is about 4 μm ± 0.05.

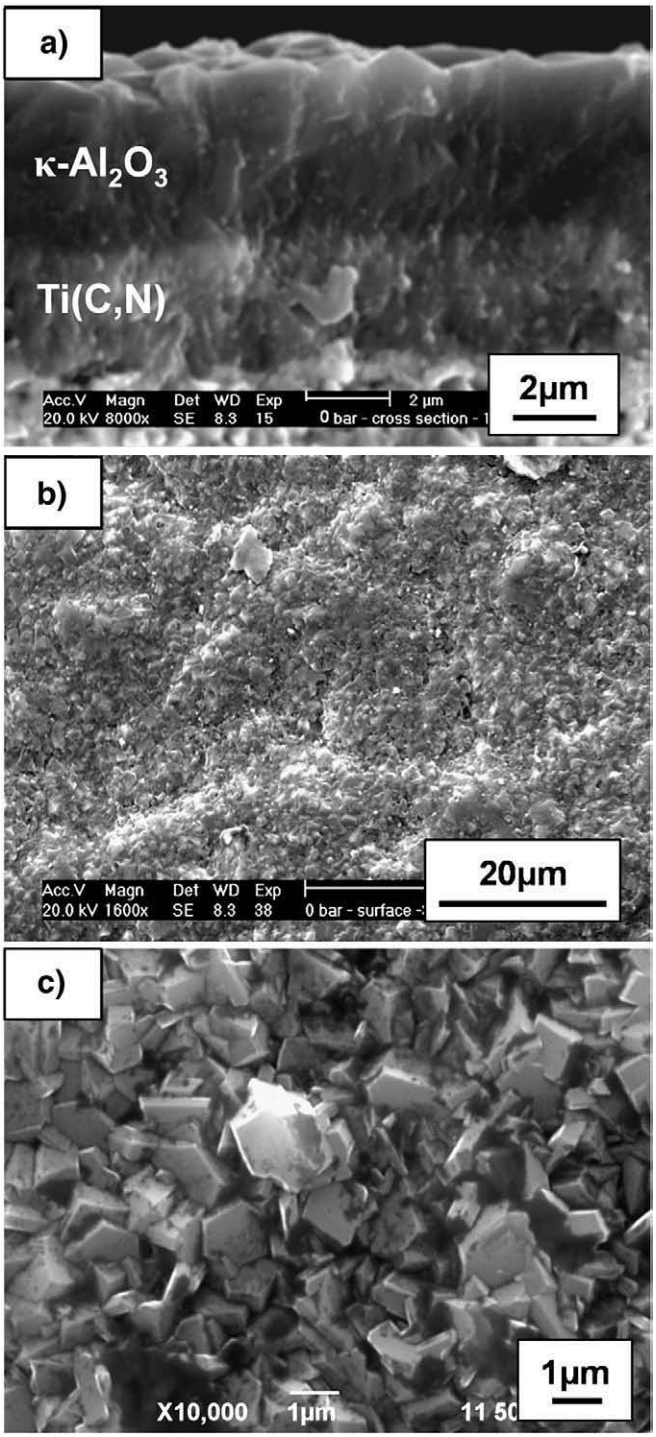

Fig. 1. SEM images of (a) fracture cross-section of the coated cemented carbide, (b) top view of the surface topography of as-deposited CVD κ-Al_2O_3 coating and (c) higher magnification (top view) of the surface topography showing hexagonal-shaped grains.

The alumina layer is composed of columnar grains that grow directly from the nucleation surface (here, the intermediate Ti(C,N) layer). The length of the columnar grains is mostly equivalent to the thickness of the alumina layer. A change in the morphology towards the surface can be observed, with the formation of hexagonal-shaped grains (Fig. 1b and c). Some cracks (mainly transgranular) can also be observed. They are typical cracks as a consequence of the different thermal expansion coefficients between the substrate and the coating and cannot really be avoided in commercial CVD cutting inserts. Several isolated large grains with average diameter larger than 5 µm

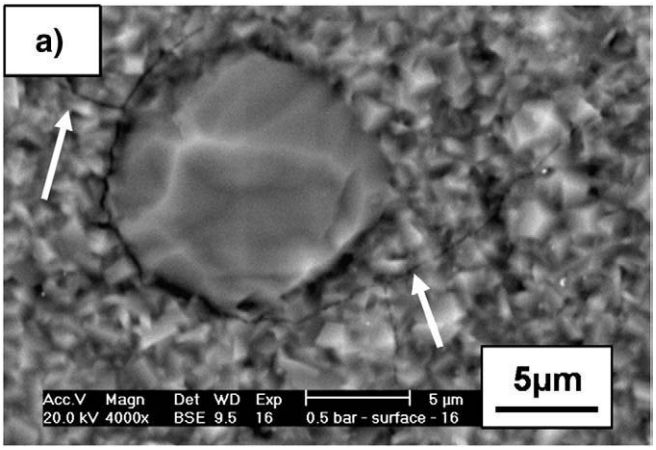

Fig. 2. SEM image (BSE mode) of κ-Al_2O_3 surface topography (top view) after coating. Isolated large Al_2O_3 grains (with average size of 5 µm) form in a random distribution throughout the surface. Crack initiation seems to be associated with these large grains (see arrows around the large Al_2O_3 grain).

formed as a single crystal or a polycrystalline structure in a random distribution throughout the surface (Fig. 2). Their number increases towards the edge of the inserts. Crack initiation seems to be associated with these outgrowths. The average surface roughness R_a measured was 0.110 ± 0.008 (Table 1).

The penetration depth of the X-rays in alumina is about 18 µm. Hence, we have full penetration of the radiation into the coating system. The X-ray diffraction (XRD) patterns for the as-deposited sample are shown in Fig. 3. The contribution of the substrate is also registered, indicated by the peaks associated with WC reflections. The XRD measurements also reveal that the intermediate layer is composed of Ti ($C_{0.3}N_{0.7}$). The intensity ratio between peaks shows no marked texture in the layers. Although the observation of the κ-→α-Al_2O_3 phase transformation already during the deposition process is generally reported in literature [29], there is no evidence for the occurrence of such transformation, since the XRD diffractograms only revealed reflections associated with κ-Al_2O_3. This indicates that the superficial cracks observed in the as-deposited coatings arise upon cooling due to the differences in thermal coefficient between the coating and the substrate, and not originating from volume contraction that occurs in phase transformation.

Fig. 4 shows a STEM micrograph of the as-deposited coating. The darkest areas at the bottom correspond to the cemented carbide substrate (WC grains are seen in black). The TiN layer with a thickness of 0.5 µm lies adjacent to the substrate. Onto the TiN layer, the Ti(C,N) layer shows a changing grain morphology (Fig. 4), making it appear as two distinct structures. The first sub-layer consists of columnar grains with a width of about 0.1 µm. The following sub-layer has significantly smaller grains with a needle-like morphology and appears randomly oriented. The uppermost layer consists of κ-Al_2O_3 (in lighter contrast) and shows grains grown along the CVD deposition direction perpendicular to the substrate. The columnar microstructure is typical

Table 1
Values of R_a, R_z and thickness for the κ-Al_2O_3 top layer as a function of micro-blasting pressure.

Micro-blasting pressure [MPa]	R_a roughness [µm]	R_z roughness [µm]	Thickness [µm]
0	0.110 ± 0.008	0.690 ± 0.04	4.20 ± 0.05
0.05	0.096 ± 0.005	0.540 ± 0.04	4.20 ± 0.05
0.1	0.079 ± 0.006	0.480 ± 0.04	4.00 ± 0.05
0.15	0.038 ± 0.004	0.190 ± 0.03	3.40 ± 0.05
0.2	0.045 ± 0.003	0.250 ± 0.03	3.00 ± 0.05
0.25	0.074 ± 0.004	0.440 ± 0.03	2.50 ± 0.05
0.3	0.084 ± 0.004	0.540 ± 0.04	2.50 ± 0.05

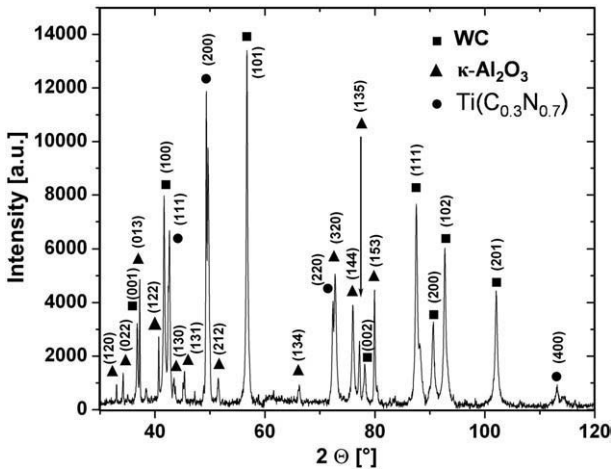

Fig. 3. X-ray diffractogram of the as-deposited κ-Al_2O_3/Ti(C,N) coatings taken at $\psi = 0°$ with synchrotron radiation energy of 6.9 keV ($\lambda_{Co} = 1.7904$ Å). The arrow indicates the position of the κ-Al_2O_3 (135) reflection used for the residual stress evaluation.

for coatings deposited at low gas pressures and low temperatures compared to the melting point temperature [30].

Besides the STEM mode, conventional Bragg diffraction contrast TEM was applied to investigate the evidence of defects within the κ-Al_2O_3 top layer. A TEM micrograph in bright field (BF) mode is shown in Fig. 5a. No dislocations but a high concentration of planar defects (twin-related faults) were observed (Fig. 5a). All obtained electron diffraction patterns

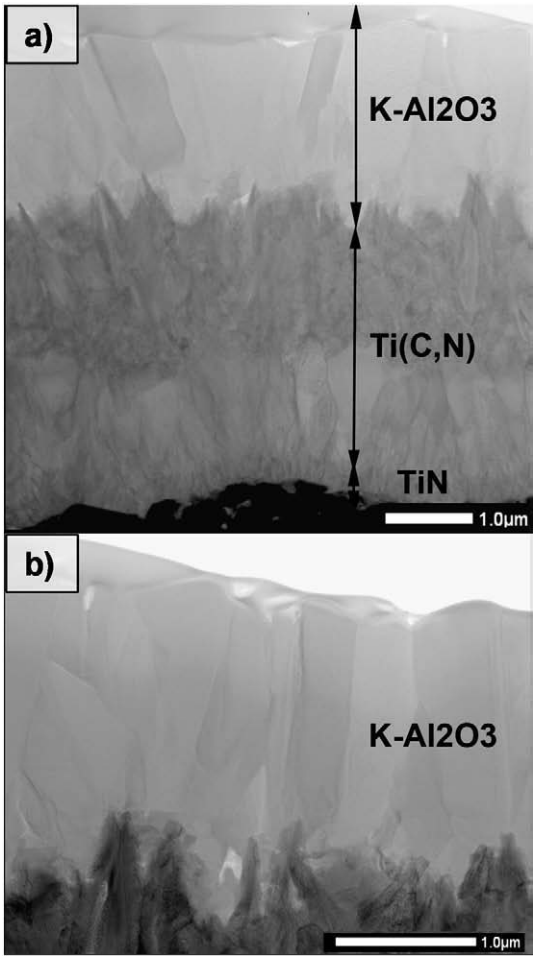

Fig. 4. (a) STEM micrograph showing the cross-section microstructure of the as-deposited coating. (b) Higher magnification of the top κ-Al_2O_3 layer.

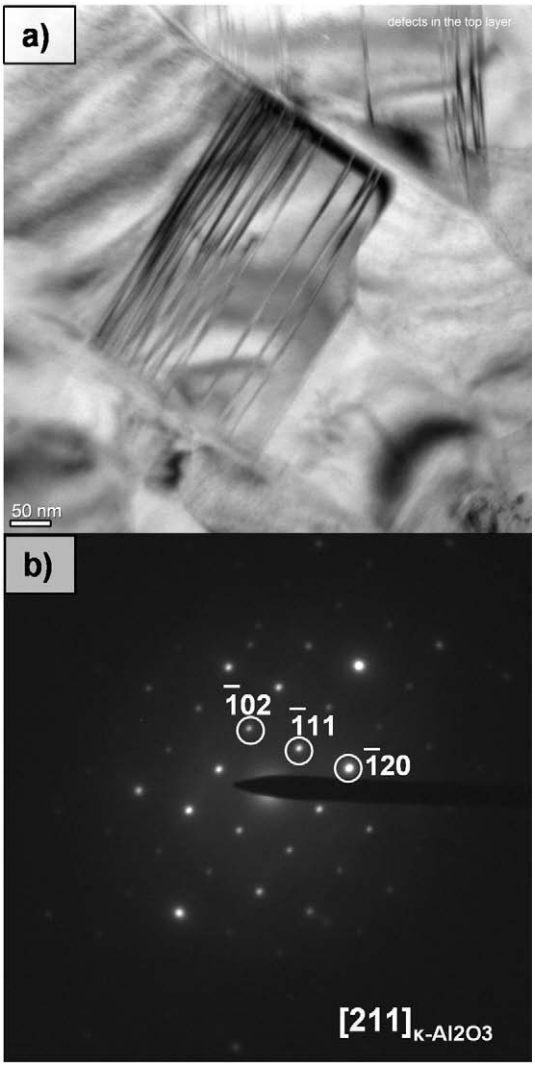

Fig. 5. TEM micrograph in bright field (BF) mode showing planar defects within the as-deposited κ-Al_2O_3 layer. (b) Selected area diffraction pattern (SADP) corresponding to κ-Al_2O_3.

(e.g. Fig. 5b) only reveal the presence of the κ-Al_2O_3 phase. No evidence of phase transformation was obtained. The two possible variations of alumina (i.e. the metastable κ-Al_2O_3 and the stable polymorph α-Al_2O_3) have strikingly different symmetry, which could have been easily distinguished if the latter were present. EDX analysis reveals almost no chemical intermixing, which suggests good separation of the layers.

3.2. Microstructure of micro-blasted coatings

Micrographs of surface morphology and fracture cross-section of the samples micro-blasted at pressures in the range 0.05–0.15 MPa are presented in Fig. 6. Lower micro-blasting pressures, i.e. 0.05 and 0.1 MPa cause no significant changes in grain morphology, although a decrease in the average roughness is measured. At blasting pressures as low as 0.05 MPa few isolated areas already appear deformed. As from 0.15 MPa, significant loss of coating material begins to occur and the number of cracks increases. Crack propagation typically occurs in a transgranular mode, but seems to be confined to the near-surface zone of the upper coating.

Micro-blasting at 0.2 MPa causes a flattening of the grains and flaking of the coating as a consequence of the strong abrasive effect due to micro-blasting (Fig. 7). Higher micro-blasting pressures (0.25 and 0.3 MPa) lead to strong changes in the surface micro-topography

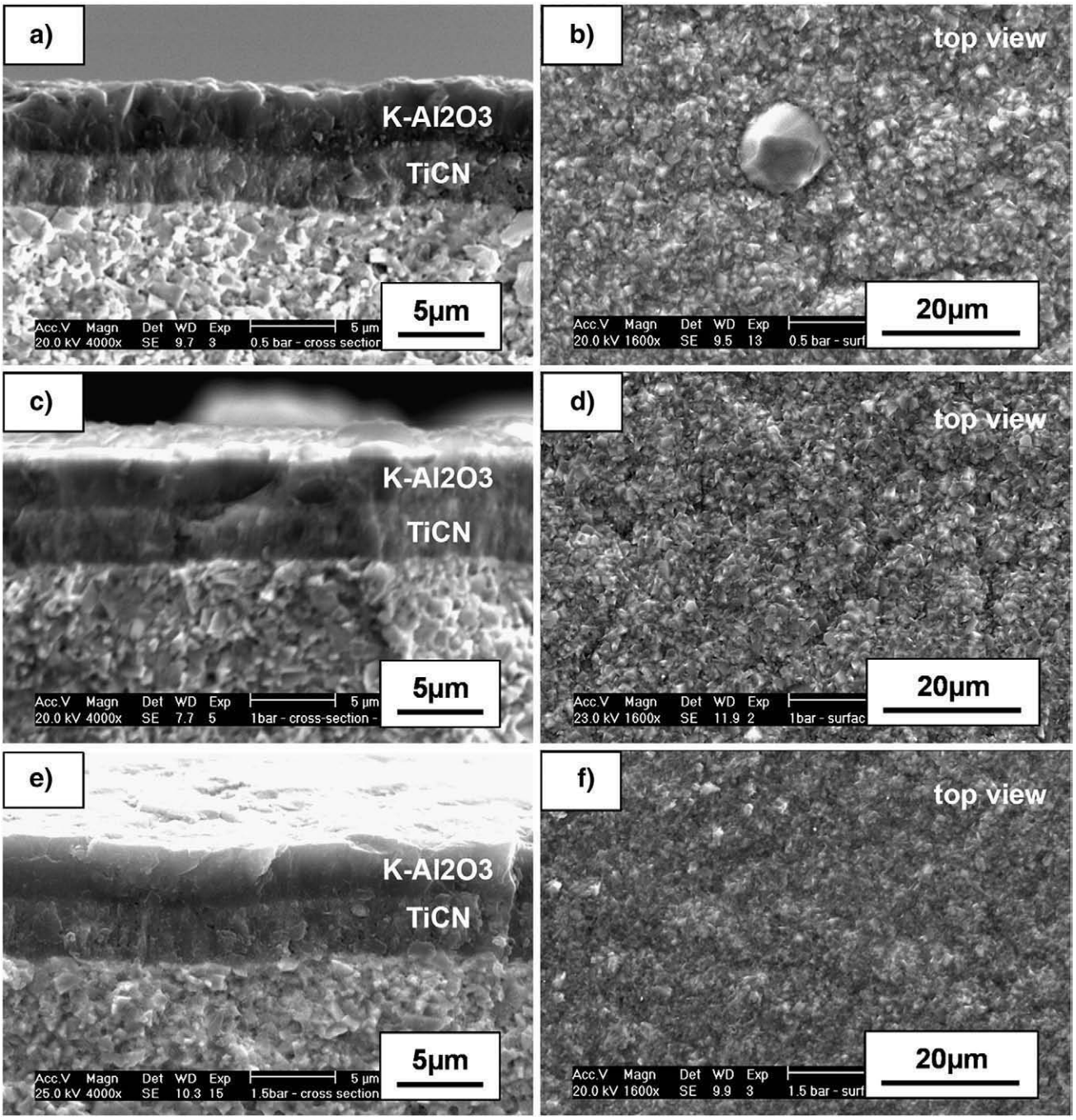

Fig. 6. SEM micrographs showing the changes on the κ-Al_2O_3 thickness (fracture cross-sections) and surface topography (top view images) as a function of micro-blasting pressure: (a) and (b) at 0.05 MPa; (c) and (d) at 0.1 MPa; (e) and (f) at 0.15 MPa.

and an increase in the number and length of the cracks. The microstructure of the Ti(C,N) intermediate layer does not seem affected by the impact of the alumina shots.

STEM micrographs of the cross-section microstructure of coatings micro-blasted at 0.1 MPa and 0.3 MPa are shown in Fig. 8. By comparing the microstructure of the micro-blasted samples at different conditions, the only difference corresponds to the significant reduced thickness of the alumina layer micro-blasted at 0.3 MPa. The influence of micro-blasting pressure on the thickness of the κ-Al_2O_3 layer is shown in Table 1. On the other hand, the results clearly show that the micro-blasting does not affect the adherence of the layer. Moreover, the Ti(C,N) is not affected by the mechanical treatment, the reduction in layer thickness being confined to the top alumina layer.

The TEM micrograph in BF mode (Fig. 8c) shows the typical planar defects also observed within the alumina layer of the micro-blasted coatings (here we only show the example of the sample micro-blasted at 0.3 MPa). The concentration of the twin-related faults observed in samples in all conditions seems to be identical, which directly suggests that the micro-blasting process has no influence on the defect density observed in the top κ-Al_2O_3 layers. Besides, not a single dislocation was observed in the analyzed micro-blasted top κ-Al_2O_3 layers.

Micro-blasting leads to a decrease in the roughness of the alumina coating, showing a minimum at blasting pressures between 0.15 and 0.2 MPa (Table 1). Increasing the blasting pressure above 0.2 MPa increases the roughness due to deterioration of the coating layer. This

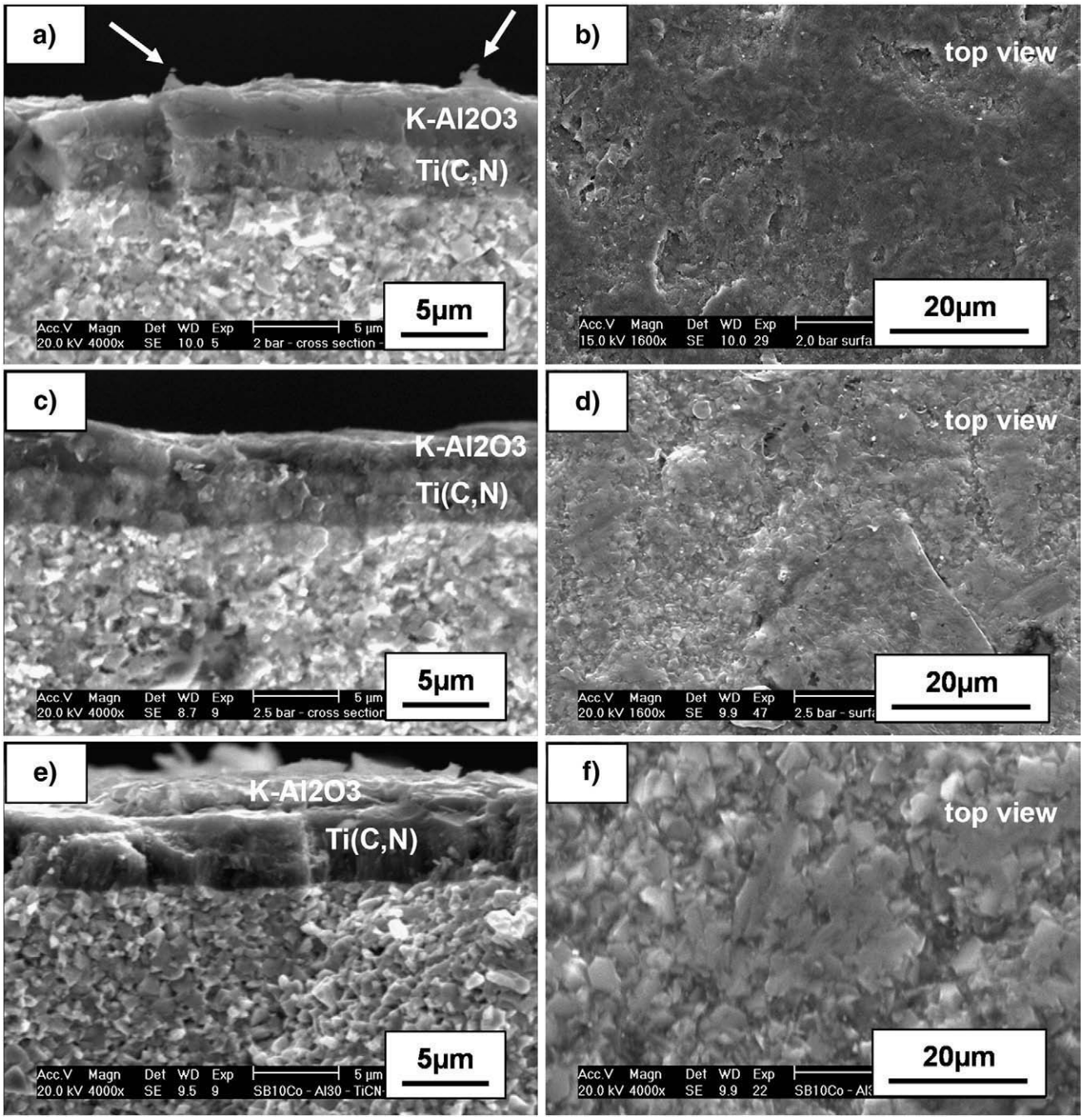

Fig. 7. SEM micrographs showing the changes on the κ-Al_2O_3 thickness (fracture cross-sections) and surface topography (top view images) as a function of micro-blasting pressure: (a) and (b) at 0.2 MPa; (c) and (d) at 0.25 MPa; (e) and (f) at 0.3 MPa.

is related to the extensive loss of the top layer material that occurs with increasing pressures. The removal of top coating material causes an increase in the line intensity of the WC reflections, since more contribution from the substrate is being registered (Fig. 9). No changes in the intensity ratio between peaks with increasing micro-blasting pressures are observed.

3.3. Residual stress analyses

The $\sin^2\psi$ curves of the κ-Al_2O_3 layers in the as-deposited and micro-blasted (at 0.1 and 0.3 MPa) conditions are presented in Fig. 10. The obtained d–$\sin^2\psi$ distributions are shown to be linear with positive slopes up to $\sin^2\psi \sim 0.92$ in all conditions, indicating the presence of average residual stresses of tensile nature within the κ-Al_2O_3 layer, which still predominate in the micro-blasted state. On top of the coatings (at large ψ angles, thus, at small penetration depths), however, the d_ψ^{hkl}–$\sin^2\psi$ distributions tend to curve downwards, suggesting the presence of near-surface gradients of the in-plane residual stresses in the as-deposited as well as in the micro-blasted conditions. ψ-splitting in the d_ψ^{hkl}–$\sin^2\psi$ plots does not occur, indicating the absence of shear stress components in all cases investigated.

The in-plane residual stresses averaged over the entire κ-Al_2O_3 layer are 355 ± 41 MPa, 349 ± 45 MPa, and 392 ± 39 MPa in the as-deposited, 0.1 and 0.3 MPa conditions, respectively (Table 2). Based on the $\sin^2\psi$ distributions (Fig. 10), the in-depth distribution of the residual stresses in the κ-Al_2O_3 coatings was determined using Eq. (1). The stress-depth profiles for the as-deposited and micro-blasted coatings are similar as presented in Fig. 11. In the as-deposited state,

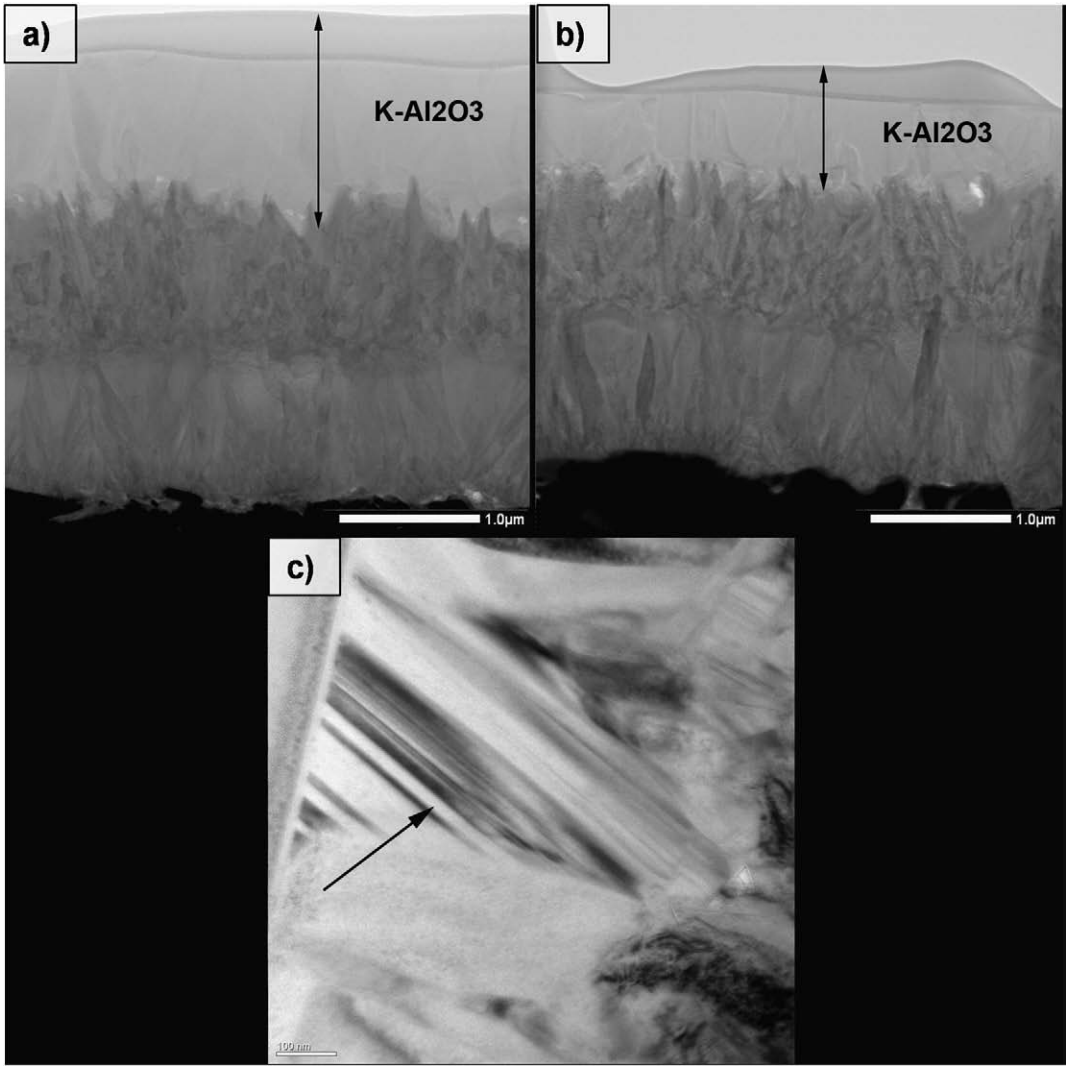

Fig. 8. STEM micrographs showing the cross-section microstructure of coatings micro-blasted at (a) 0.1 MPa and (b) 0.3 MPa. (c) TEM micrograph (BF) showing planar defects within the alumina layer of the coating micro-blasted at 0.3 MPa.

the residual stress in the 'bulk' of the layer was found to be $\sigma_{//}(\tau \approx 1.5\ \mu m) = 699$ MPa, whereas the obtained value at the outer surface decreases down to $\sigma_{//}(\tau \approx 0) = -32$ MPa. This indicates that the stresses become gradually less tensile towards the free surface, eventually turning into low compression at the surface. A similar behaviour is observed for the specimen micro-blasted at 0.1 MPa: the tensile residual stress within the coating is slightly lower $\sigma_{//}(\tau \approx 1.5\ \mu m) = 603$ MPa, whereas at the surface low compressive residual stresses $\sigma_{//}(\tau \approx 0) = -42$ MPa are also obtained. For the specimen micro-blasted at 0.3 MPa, the stress values are $\sigma_{//}(\tau \approx 1.5\ \mu m) = 546$ MPa and $\sigma_{//}(\tau \approx 0) = 153$ MPa within the coating and close to the surface, respectively (Table 2).

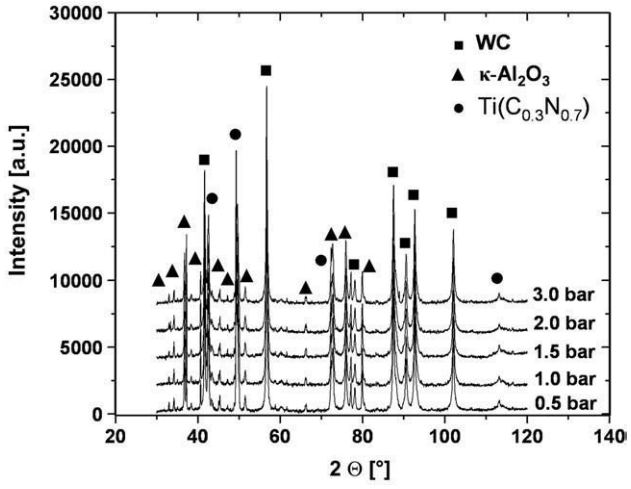

Fig. 9. X-ray diffractograms of micro-blasted coatings as a function of micro-blasting pressure showing no change in the intensity ratio between peaks with increasing micro-blasting pressures.

The analysis of the average integral breadth of the {135} diffraction line of κ-Al_2O_3 suggests that the density of lattice imperfections does not significantly increase with increasing micro-blasting pressures. This information corroborates the TEM investigations, which reveal low dislocation densities, even with increasing micro-blasting pressures.

4. Discussion

4.1. Effect of micro-blasting on microstructure and roughness

Our results indicate that the micro-blasting procedure only affects the κ-Al_2O_3 top coating layer. SEM and TEM images show that there are no disturbances in the integrity of the intermediate Ti(C,N) layer.

Strong deformation of the coatings appears as a flattening effect on the near-surface zone, mainly at pressures higher than 0.1 MPa. This

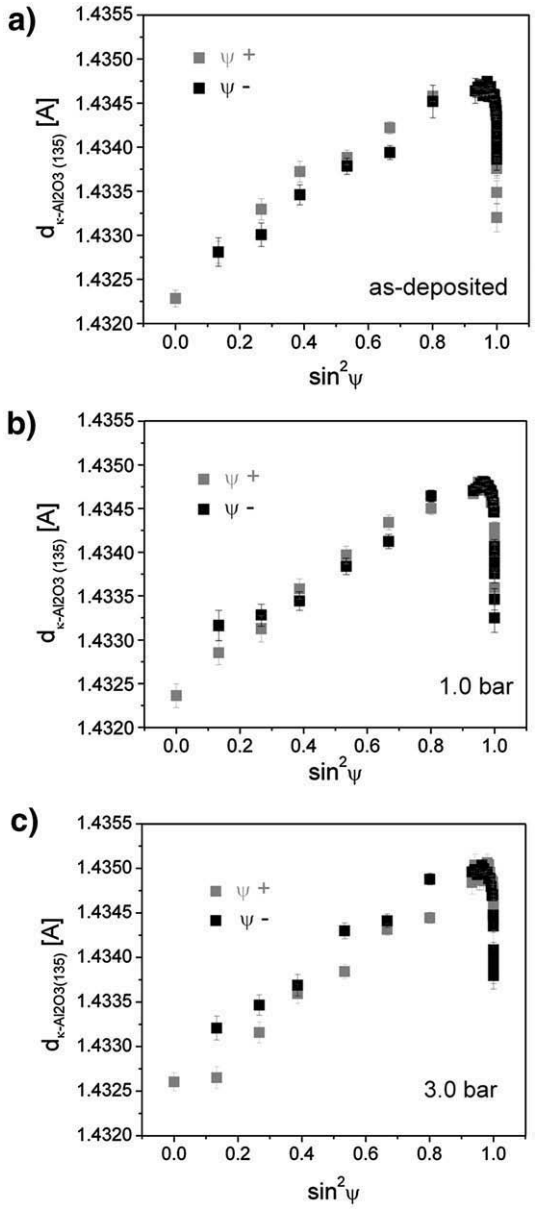

Fig. 10. The $\sin^2\psi$ distributions of the κ-Al_2O_3 (135) reflection for $\varphi = 0°$ of the coatings (a) as-deposited, (b) micro-blasted at 0.1 MPa and (c) micro-blasted at 0.3 MPa.

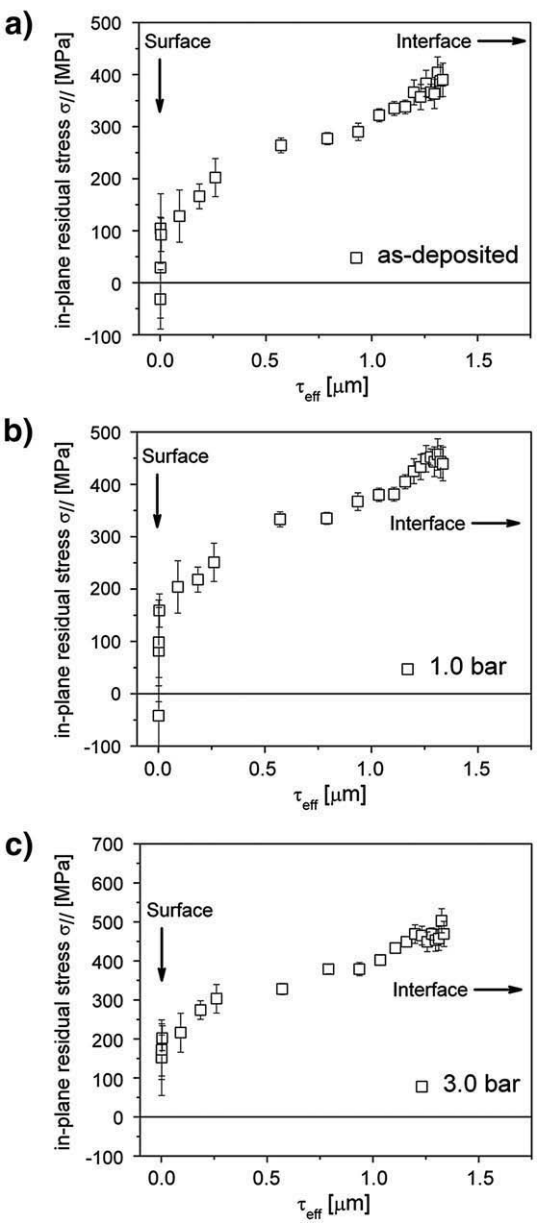

Fig. 11. Depth profile of the in-plane residual stresses obtained from the evaluation of the $\sin^2\psi$ distributions shown in Fig. 11 for the coatings (a) as-deposited, (b) micro-blasted at 0.1 MPa and (c) micro-blasted at 0.3 MPa.

flattening is produced on the one hand by the overlapping of the several localized deformations caused by the impact of the alumina shots on the surface. On the other hand, the impacts also remove material from the alumina coating, which also results in a smoothing of the protruding irregularities on the surface (Table 1). The lower roughness in the contact zone of the coating decreases the mechanical contact between asperities of the tribological pair tool-workpiece. This leads to a lower friction coefficient and thus, a contribution for extended tool life of the inserts.

Table 2
Values of internal stresses in the κ-Al_2O_3 top layer as a function of micro-blasting pressure.

Micro-blasting pressure [MPa]	Average in-plane residual stresses [MPa]	Stress value near the outer surface of κ-Al_2O_3 [MPa]	Stress value in the "bulk" of κ-Al_2O_3 [MPa]
0	355 ± 41	$\sigma_{//}(\tau \approx 0) = -32$	$\sigma_{//}(\tau \approx 1.5\ \mu m) = 699$
0.1	349 ± 45	$\sigma_{//}(\tau \approx 0) = -42$	$\sigma_{//}(\tau \approx 1.5\ \mu m) = 603$
0.3	392 ± 39	$\sigma_{//}(\tau \approx 0) = 153$	$\sigma_{//}(\tau \approx 1.5\ \mu m) = 546$

4.2. Origin of stresses and defects

4.2.1. Stress development upon CVD deposition

CVD coatings are known to evolve relevant thermal mismatch residual stresses upon cooling from the high deposition temperatures [31]. The strain and stress state in the layers change due to thermal strain introduced by differences in the coefficients of thermal expansion between the individual layers and the substrate. The maximum thermal stresses induced by cooling (without taking stress relieving processes into account) can be estimated by using the Dietzel equation [32]:

$$\sigma_c = \{E_c(\alpha_c - \alpha_s)\Delta T\} / (1 - \nu_c) + \{[(1 - \nu_s) / E_s]d_c / d_s\} \quad (3)$$

where α is the linear coefficient of thermal expansion, ν is the Poisson ratio, E is the Young's modulus, d is the thickness, c stands for coating and s for substrate. The thermal expansion coefficient (TEC)

of κ-Al_2O_3 and Ti(C,N) usually lies within 8.0–9.0 × 10^{-6} K^{-1} [33], whereas in the case of WC–Co cemented carbides it is in the range within 4.0–7.0 × 10^{-6} K^{-1} depending on the composition [34]. Hence, tensile stresses will necessarily develop in the κ-Al_2O_3 coating since $\alpha_{\kappa\text{-}Al2O3} > \alpha_s$. Our results clearly show that average tensile stresses develop within the κ-Al_2O_3 layer, indicating that thermal strains represent the major source of residual stresses in the present case. The low compressive stress values towards the surface could be attributed to the relaxation of the tensile residual stresses existent in the 'bulk' of the layer, since the interaction between the substrate and the coatings tends to decrease when approaching the free surface. Besides, the crack propagation, which seems to be confined to the zone closest to the surface, might also play a role in the relaxation mechanism.

4.2.2. Stresses and defects induced by micro-blasting

The residual stresses are generally classified into three types: macro-stresses, micro-stresses, and root mean square (r.m.s.) stresses [25]. Macro-stresses often develop during sample manufacturing, extending homogeneously over macroscopic distances, i.e. several grains. In contrast, micro-stresses arise over microscopic volumes, typically grain sizes, due to the mismatches in thermal and mechanical properties of the individual phases or grain orientations. Both cause diffraction line shifts since they are related to average lattice strains of grains with specific orientations. As discussed in the Section 4.2.1, they are of thermal origin in the present case, and are not affected by the applied micro-blasting treatment.

The third type of stresses (r.m.s. stresses), which is inhomogeneous within subgrains or crystallites due to the presence of lattice imperfections and vary on the atomic scale, does not induce line shifts but only diffraction line broadening, since any disturbance in the regularity of the crystal lattice is reflected in lattice parameter fluctuations. Typical causes for diffraction line broadening are therefore lattice distortions that arise from crystal defects (e.g. dislocations and planar faults), changes in the diffraction coherence length (domain size) and domain-size distribution [28].

Based on evidences provided by both TEM and XRD investigations, we conclude that the κ-Al_2O_3 top layer does not undergo plastic deformation during micro-blasting. In particular, TEM imaging indicates practically the absence of dislocations, even at a micro-blasting pressure as high as 0.3 MPa, which promotes extensive loss of the κ-Al_2O_3 layer and strong changes in layer micro-topography. Planar defects in the form of twin-related faults are the only type of crystalline defects observed and already predominate in the as-deposited state, the density of which is not affected by the micro-blasting process.

The crystal structure of the metastable κ-Al_2O_3 is well established. It has an orthorhombic crystal structure (space group $Pna2_1$) with lattice parameters $a = 4.844$ Å, $b = 8.330$ Å, $c = 8.955$ Å formed from a pseudo-closed-packed stacking ABAC of oxygen atoms with Al in octahedral and tetrahedral environments in a 3:1 ratio [35,36]. Supposedly, due to the rather complex crystalline structure, distortion of the lattice occurs differently according to the crystallographic direction leading to twinning as the predominant deformation mechanism in κ-Al_2O_3 phase in contrast to α-Al_2O_3, in which dislocation is the type of recurrent defects observed.

5. Conclusions

Micro-blasting at pressures ranging from 0.05 up to 0.3 MPa was applied to CVD κ-Al_2O_3/Ti(C,N)/TiN multilayer coatings in order to investigate the potentiality of this procedure to control the surface micro-topography and modify the residual stress state of the coating. Our investigations reveal that:

1. The κ-Al_2O_3 growth occurs in columnar direction, perpendicular to the substrate. No κ → α phase transformation of the Al_2O_3 is induced by micro-blasting according to both synchrotron X-ray diffraction and TEM studies.
2. The effects of the micro-blasting treatment on the TiN/Ti(C,N)/κ-Al_2O_3 multilayer under the conditions investigated are confined to the κ-Al_2O_3 top layer, as revealed by the TEM and STEM investigations.
3. Increasing the micro-blasting pressure leads to the formation and propagation of cracks. SEM and TEM investigations show that crack propagation is confined to the zone closest to the surface.
4. Increasing micro-blasting pressure leads to a reduction in roughness from R_a: 0.110 ± 0.008 / R_z: 0.690 ± 0.04 in the as-deposited coatings up to R_a: 0.038 ± 0.004 / R_z: 0.190 ± 0.03 in coatings micro-blasted at 0.15 MPa, which is mainly associated with the loss of coating material. Blasting pressures above 0.2 MPa lead to coating degradation.
5. TEM investigations showed high density of planar defects in the κ-Al_2O_3 in the form of twin-related faults (Figs. 5 and 8). TEM and XRD investigations reveal that the κ-Al_2O_3 top layer does not undergo plastic deformation during micro-blasting.
6. The residual stresses are of tensile nature and thermally induced and are not affected by the applied micro-blasting treatment. The average stress values over the κ-Al_2O_3 layer are 355 ± 41 MPa, 349 ± 45 MPa, and 392 ± 39 MPa in the as-deposited, 0.1 MPa and 0.3 MPa conditions. These tensile stresses ease towards the free surface.

It can be in general concluded that, under the conditions investigated, the more remarkable effect of the micro-blasting treatment on the κ-Al_2O_3 top layer was a reduction of the surface roughness for blasting pressures up to 0.15 MPa and a strong coating degradation for blasting pressures above 0.2 MPa. Neither the morphology nor the residual stress state of the κ-Al_2O_3 top layer was affected by the micro-blasting. This is a main difference in the response to the treatment compared with the reported values for α-Al_2O_3 [22,24,26], pointing out that the generation of compressive internal stresses by micro-blasting depends strongly on the crystalline structure of the Al_2O_3 phase. This observation may be supported by previous investigations indicating a higher degree of plasticity of α-Al_2O_3 [37] compared to κ-Al_2O_3. On the other hand, the different physical characteristics of the metastable CVD κ-Al_2O_3 compared to the CVD α-Al_2O_3, such as a smaller grain size, a lower pore density and an epitaxial growth, may also have an influence on the internal stress conditions after micro-blasting treatment [35].

Acknowledgements

The authors (J. Garcia and H. Pinto) thank the financial support of the DFG project 444Bra-113/25/0-1 to carry out part of this work. Anna di Prinzio thanks ADEMAT Network, Alfa-project Nr. II-0240-B1-AT-RT-CT for financial support. Dr. A. Rothkirch (Hasylab), Dr. C. Juricic and Mr. P. Brito (MPIE) are kindly acknowledged for their support during the synchrotron X-ray measurements. Thanks to Mr. U. Föckeler (Ruhr Universität Bochum) for atom force microscopy measurements.

References

[1] F. Bunshah, Handbook of Hard Coatings, Noyes Publications/William Andrew Publishing, LLC, Norwich, New York, USA, 2001.
[2] P.K. Mehrothra, D.T. Quinto, High Temp. High Press. 18 (1980) 199.
[3] B.M. Kramer, N.P. Suh, J. Eng. Ind. 102 (1980) 303.
[4] R.H. French, J. Am. Ceram. Soc. 73 (1990) 477.
[5] B. Holm, R. Ahuja, Y. Yourdshhyan, B. Johansson, B.I. Lundqvist, Phys. Rev., B 59 (1999) 12777.
[6] S. Ruppi, Int. J. Refract. Met. Hard Mater. 23 (2005) 306.
[7] S. Ruppi, A. Larsson, Thin Solid Films 388 (2001) 50.
[8] S. Ruppi, A. Larsson, A. Flink, Thin Solid Films 516 (2008) 5959.
[9] H. Holzschuh, Patent US 6,436,519 B2, 20.08.2002.
[10] H. Halvarsson, S. Vuorinen, Surf. Coat. Technol. 56 (1993) 165.
[11] M. Halvarsson, H. Nordén, S. Vuorinen, Surf. Coat. Technol. 68–69 (1994) 266.
[12] M. Halvarsson, J.E. Trancik, S. Ruppi, Int. J. Refract. Met. Hard Mater. 24 (2006) 32.
[13] R. Pitonak, J. Garcia, R. Weissenbacher, K. Udier, Patent EP 1948842, 30.07.2008.
[14] D.M. Kennedy, J. Vahey, D. Hanney, Mater. Des. 26 (2005) 203.
[15] J. Qu, A.J. Shih, R.O. Scattergood, J. Luo, J. Mater. Process. Technol. 166 (2005) 440.

[16] K.-D. Bouzakis, N. Michaidilis, G. Skordaris, S. Kombogiannis, S. Hadjiyiannis, K. Efstathion, G. Erkens, S. Rambadt, I. Wirth, CIRP Ann. — Manufacturing Technol. 51 (2002) 61.
[17] H.K. Tönshoff, H. Seegers, Thin Solid Films 377–378 (2000) 340.
[18] K.-D. Bouzakis, N. Michailidis, S. Hadjiyiannis, K. Efstathiou, E. Pavlidou, G. Erkens, S. Rambadt, I. Wirth, Surf. Coat. Technol. 146–147 (2001) 443.
[19] K.-D. Bouzakis, N. Michailidis, J. Anastopoulos, S. Kompogiannis, G. Erkens, P.J. Roudnik, Surf. Coat. Technol. 153 (2002) 148.
[20] K.-D. Bouzakis, G. Skordaris, I. Mirisidis, N. Michailidis, G. Mesomeirs, E. Pavlidou, G. Erkens, Surf. Coat. Technol. 200 (2005) 1879.
[21] F. Klocke, T. Schroeder, E. Bouzakis, A. Klein, Surf. Coat. Technol. 202 (4–7) (2007) 1194.
[22] H. Westphal, V. Sottke, Patent DE 10123554 A1, 22.12.2002.
[23] S. Ruppi, Patent US 6,015,614, 18.01.2000.
[24] H. Holzschuh, Patent US 2008/0050614 A1, 28.02.2008.
[25] V. Hauk, Structural and Residual Stress Analysis by Nondestructive Methods, Elsevier, Amsterdam, 1997 Chapter 2.072.
[26] M. Klaus, Ch. Genzel, H. Holzschuh, Thin Solid Films 517 (3) (2008) 1172.
[27] Ch. Genzel, Mater. Sci. Technol. 21 (2005) 10.
[28] E.J. Mittemeijer, P. Scardi, Diffraction Analysis of the Microstructure of Materials, Springer Verlag Berlin-Heidelberg, Germany (2004).
[29] S. Vuorinen, J. Skogsmo, Thin Solid Films 193 (1990) 536.
[30] M. Panjan, S. Sturm, P. Panjan, M. Cekada, Surf. Coat. Technol. 202 (4–7) (2007) 815.
[31] D.T. Quinto, Int. J. Refract. Met. Hard Mater. 14 (1–3) (1996) 7.
[32] H. Salmang, H. Scholze, Keramik. Teil I, Springer, Berlin (1982) p.237.
[33] C. Friedrich, G. Berg, E. Broszeit, C. Berger, Materialwiss. Werkstoff. 28 2 (2004) 59.
[34] R. Kieffer, F. Benesovsky, Hartmetalle, Springer Verlag, Wien, New York, 1965.
[35] Y. Yourdshahyan, C. Ruberto, M. Halvarsson, L. Bengtsson, V. Langer, B. Lundqvist, S. Ruppi, U. Rolander, J. Am. Ceram. Soc. 82 (6) (1999) 1365.
[36] B. Ollivier, R. Retoux, P. Lacorre, D. Massiot, G. Férey, J. Mater. Chem. 7 (1997) 1049.
[37] S. Ruppi, M. Halvarsson, Thin Solid Films 353 (1999) 182.